DOI: https://doi.org/10.68732/bcb6854b02a2e67c

ISBN: 978-9989-2053-6-1

Phase-field fracture simulation for strain rate effect on fracture propagation

A. Chehreh, LC. Witte, M. Duda & T. Backers
Ruhr University Bochum, Bochum, Germany
hossein.asgharichehreh@ruhr-uni-bochum.de

Abstract

For the spatial and temporal upscaling of results from uniaxial compressive strength tests on rocks, numerical methods are necessary to predict rock behaviour under complex geomechanical conditions, as in foundation, slope stability, underground space, and reservoir studies. Correctly estimating the impact of time and scale on parameters can lead to reduced design risk. Previous studies on phase-field modelling of rocks often employed a single open flaw to simulate fracture initiation, and two to four open flaws to represent fracture propagation and failure. These flaws were generally arranged in a geometrically ordered pattern. However, in natural rock formations, microfractures are predominantly closed and exhibit a random distribution depending on texture.

This study used a phase-field approach to simulate brittle fracturing in granite containing multiple randomly distributed, closed pre-existing microcracks, employing the principal stress criterion as the driving force in the phase-field evolution equation. This study focuses on analysing the sensitivity of the model to crack density and phase-field parameters. The effect of strain rate was investigated, and phase-field parameters were calibrated accordingly.

To demonstrate the accuracy of the presented approach, numerical simulations are compared with experimentally obtained results, showing that the approach is capable of temporal and spatial upscaling when microstructural features are considered.

Keywords

Phase-field fracture, Strain rate, UCS test, Stress perturbation, Micro Cracks analysis.

1 Introduction

Predicting the failure of materials and structures due to crack nucleation and propagation is crucial for many engineering applications. As a result, several numerical frameworks have been developed to capture complex fracture phenomena. Finite element methods (FEM) are often employed in conjunction with models based on linear elastic fracture mechanics. In contrast to methods that represent cracks as discrete curves or surfaces of discontinuity, the phase-field approach (PFM) models cracks with a spatially diffuse fracture zone using an additional continuous field variable, referred to as the phase-field coefficient. This coefficient is used to degrade the material's elastic stiffness and stress-carrying capacity. The phase-field fracture approach naturally captures the emergence of complex crack patterns and behaviour, including crack nucleation, turning, branching, and intersecting in both two and three dimensions without requiring any additional constitutive assumptions. Due to this feature, phase field models have been extensively utilised to simulate an array of brittle fracture problems (Bourdin 2007), and crack growth in rock and rock-like materials (Zhao et al. 2023).

In this study, we propose a phase-field model for simulating brittle fractures developing at different externally applied strain rates in granite containing pre-existing (micro-) cracks. We applied the principal stress criterion as driving force in the evolution equation of the conventional phase-field model (CPFM) presented by Miehe (2010a) and simulated the fracture process in COMSOL Multiphysics. The terms ‘fracture’ and ‘crack’ are used synonymously.

1.1 Phase field formulation

We consider an elastic body $\Omega \subset R^d$ with $d \in \{1,2,3\}$ representing the spatial dimensions as illustrated in Fig. 2c. The external boundary and the internal discontinuity set of this elastic body are denoted as $\delta\Omega$ and Γ, respectively. The phase-field method is typically employed by integrating a variational approach, which necessitates the fracture energy ψ_f to be derived from the stored elastic energy ψ_ε (Miehe et al. 2010a). Fracture propagation can be conceptualised as a process that minimises the energy functional $\psi_{(u,\Gamma)}$ according to

$$\psi_{(u,\Gamma)} = \underbrace{\int_\Omega \psi_{(\varepsilon(\boldsymbol{u}),\varphi)}\, d\Omega}_{\psi_\varepsilon} + \underbrace{\int_\Gamma G_c\, d\Gamma}_{\psi_f} - \underbrace{\int_\Omega B_{(x,t)}.\boldsymbol{u} d\Omega - \int_{\partial\Omega_t} T_{(x,t)}.\boldsymbol{u}\, d\,\partial\Omega_t}_{W_{ext}}, \quad (1)$$

where $\boldsymbol{u}$, G_c, W_{ext}, B, T, and φ represent the displacement field, the critical strain energy release rate, the external work, the body force, the surface traction, and an auxiliary field, $\varphi(x,t) \in [0,1]$ (with x being a position vector), known as the phase field. This phase field is employed to diffuse the crack surface over the domain Ω as depicted in Fig. 2d. Consequently, in the regularised model, the phase field φ assists in smoothing out discontinuities, facilitating the numerical treatment of fractures according to

$$\varphi = \begin{cases} 0 & \text{if material is intact} \\ 1 & \text{if material is fully cracked} \end{cases}. \quad (2)$$

Then, by combining equations (1) and (2), and by substituting W_{ext} with the external crack driving stress σ_{ext}, and ψ_f with critical stress σ_c, the phase-field fracture driving force relies on the principal stress criterion concept D,

$$D = \xi \left\langle \left(\frac{\sigma_{ext}}{\sigma_c}\right)^2 - 1 \right\rangle, \quad (3)$$

where $\langle \mp \rangle$ is the Macaulay bracket, and ξ is the material factor, a dimensionless parameter greater than zero that triggers the activation of damage due to the elasto-plastic contribution and governs the post-nucleation behaviour of cracks.

1.2 Effect of phase-field parameters on simulation results

To evaluate the effects of different phase-field parameters on simulation results we performed a set of numerical simulations of uniaxial deformation experiments in a medium with two pre-existing flaws (Fig.1).

1.2.1 Critical stress $\boldsymbol{\sigma_c}$

An increase in external stress is accompanied by a gradual increase in stress at crack tips (Fig. 1a); Therefore, at a certain point, a critical stress level, $\boldsymbol{\sigma_c}$, is reached, beyond which the driving force, D,

becomes equal to 1. By decreasing the critical stress, the fracture propagation starts earlier (Fig. 1b).The critical stress $\boldsymbol{\sigma}_c$ can be determined by calibrating the crack initiation threshold ($\boldsymbol{\sigma}_{ci}$) that is assumed to be proportional to experimentally determined fracture toughness.

1.2.2 Material factor $\boldsymbol{\xi}$

With a further increase in external stress by following a particular slope, $\boldsymbol{\xi}$, according to Equation (3), the crack propagates. The high rate of fracture propagation exhibits a rapid increase for high values of $\boldsymbol{\xi}$, whereas low propagation rates are observed for small values of $\boldsymbol{\xi}$ and therefore, $\boldsymbol{\xi}$ controls the brittleness. Considering that $\boldsymbol{\xi}$ governs the behaviour of the phase field fracture following thecritical crack initiation point,σ_{ci}, it can be stated that in samples containing two or more joints (Fig. 1c), $\boldsymbol{\xi}$ can be defined by calibrating the slope of the stress-strain diagram in stable crack growth or the crack initiation stress to crack coalescence stress ratio, σ_{cd}.

1.2.3 Length scale $\boldsymbol{l_c}$

Although Miehe et al. (2010a) noted that the response of equation (3) is independent of the internal length scale, $\boldsymbol{l_c}$, determining its correct value affects the mechanical behavior of fractures by controlling the size of the regularisation zone (Fig. 1d), and the modelling cost by adjusting the finite elements mesh size (Molnar et al. 2020). According to Miehe et al. (2010b), $\boldsymbol{l_c}$ is a function of the finite element mesh size and previous studies have calculated the length scale according to the set mesh size, h_{mesh}, through $l_c \geq 2h_{\text{mesh}}$.

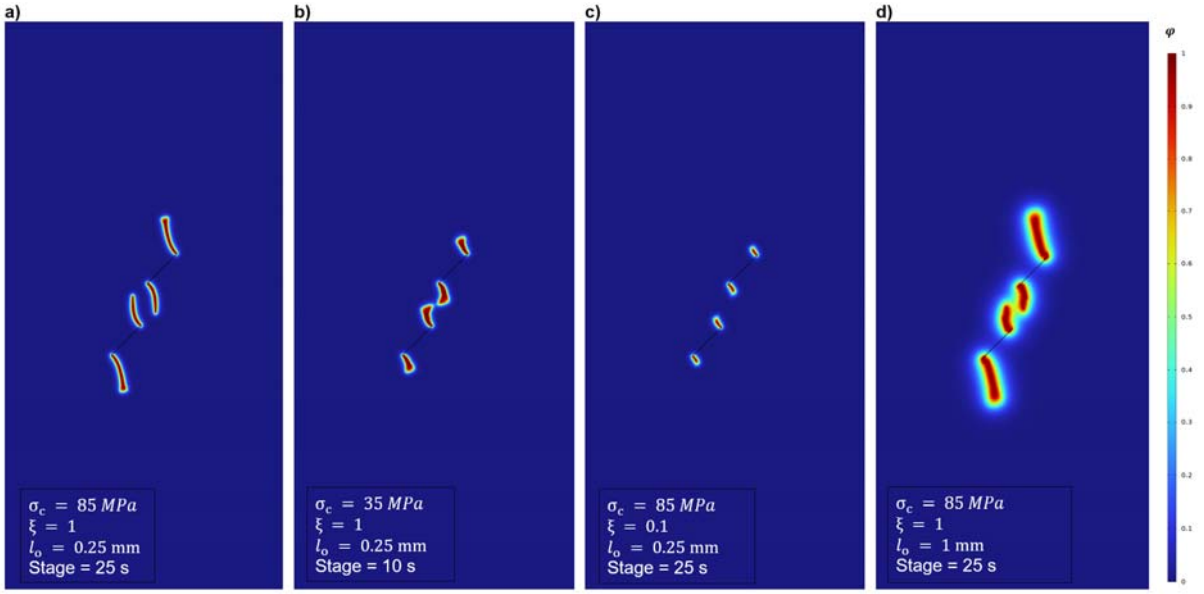


Fig. 1 Effect of phase-field coefficients on fracture propagation applying the CPFM in a numerical simulation of a uniaxial deformation experiment of a medium with two flaws with 45° inclination: (a) reference simulation, (b) effect of critical stress, (c) effect of material factor,(d) effect of length scale.

2 Material, model configuration and calibration

Numerical models were developed to replicate the laboratory experiments performed on granite specimens (samples from Padang quarry, China; Witte et al. 2025) within this study. The cylindrical specimen has an idealised dimension of 40 mm in diameter and 80 mm in length (Fig. 2a). For the time-dependent study used in CPFM, loading was applied with a controlled strain rate ranging from $1{\cdot}10^{-3}$ to $1{\cdot}10^{-6}$ s^{-1}, corresponding to a displacement rate of $0.08{\cdot}10^{-3}$ to $0.08{\cdot}10^{-6}$ mm s^{-1}. The geometric configuration of the models as well as the boundary conditions and microcracks are illustrated in Fig. 2a. Monitoring points were evenly distributed to capture a comprehensive view of the axial stress distribution. The average of these recorded values served as a representative measure of axial and lateral stress and displacement. The purpose of the calibration of the CPFM was to align its key parameters, i.e., uniaxial compressive strength (UCS) and Young's modulus, with the laboratory results. The micro-parameters of the model can be categorised into three groups, including those associated with crack geometry, i.e., crack length, L (1 mm), and crack density ($5cm^{-2}$), elastic properties of minerals, i.e., Young's modulus (55 GPa), Poisson`s ratio (0.3) and bulk density (2650 kg m^{-3}), and phase field damage parameters, i.e., critical fracture stress, σ_c (MPa), material

factor, ξ, and internal length scale, l_c (0.2 mm). The external stress, σ_{ext} (MPa), was calculated from the maximum stress at macroscopic failure. Fig. 2c shows the calibration procedure flow chart for CPFM parameters. The basic model (with a strain rate of $1 \cdot 10^{-5}$ s^{-1}) was calibrated first using the experimentally obtained micro-parameters for further modelling with different strain rates and under different boundary conditions. The results of the parameter calibration are summarised in 0.

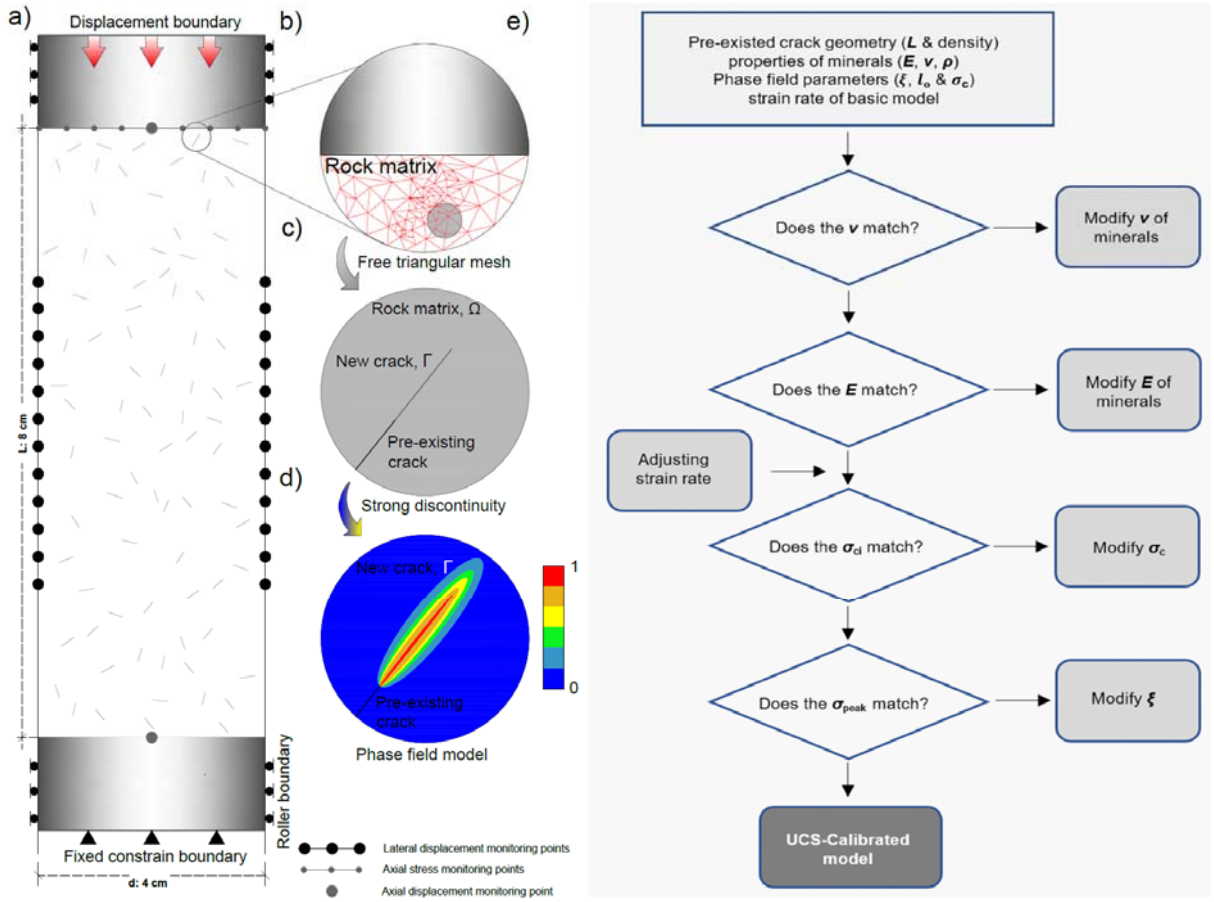


Fig. 2 (a) uniaxial compressive strength test model, (b) free triangular mesh, (c) pre-existing and new cracks in displacement field, (d) new existing crack in the phase field model, (e) flow chart of CPFM parameter calibration.

3 Simulation results

The results of the UCS basic model are depicted in Fig. 3. The CPFM effectively represents various stages of the fracturing process (c.f. Bieniawski 1967). These phases include the linear elastic response, initiation of cracks, stable crack propagation, coalescence and unstable crack propagation, and eventually macroscopic failure. However, certain aspects observed in laboratory experiments, such as crack closure and post-peak behaviour, could not be simulated. For calibration, all parameters were adapted from the basic model, with adjustments made only to the critical stress σ_c and the material factor ξ. As shown in Fig. 4 and 0, the yield stress and the number of fractures increase with increasing strain rate, while the total fracture length decreases.

Table 1. Comparison of numerical and experimental results for UCS tests at difference strain rates.

Strain rate (s^{-1})	Calibration results		Simulation results (MPa)	Experimental results (MPa)	Accuracy (%)
	Critical stress, σ_c (MPa)	Material factor, ξ (-)			
$1 \cdot 10^{-6}$	77	0.1	216	213 ± 20	98
$1 \cdot 10^{-5}$	80	0.13	227	225 ± 17	99
$1 \cdot 10^{-4}$	85	0.21	242	243 ± 18	99
$1 \cdot 10^{-3}$	100	1.8	258	259 ± 18	99

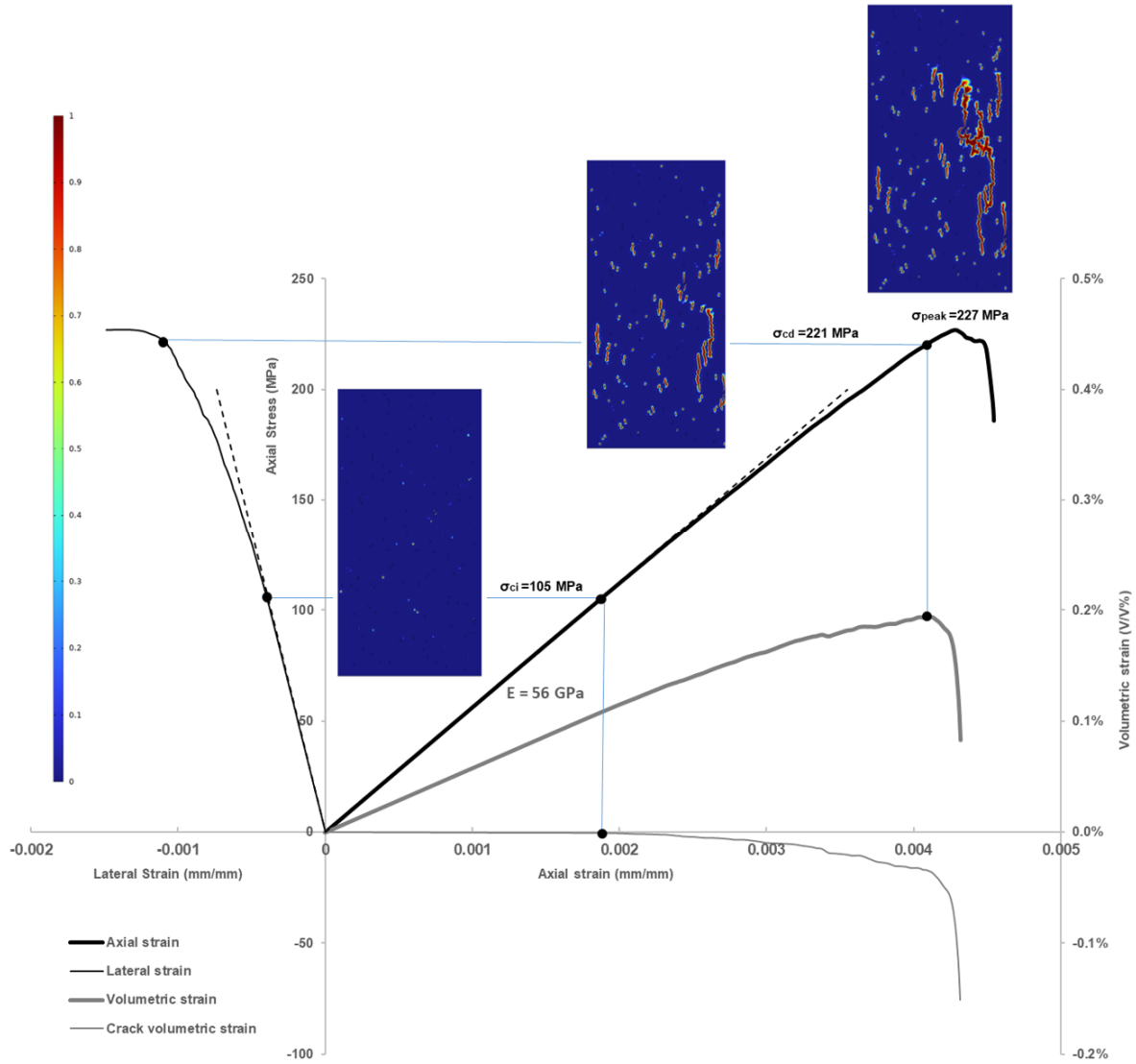


Fig. 3 Stress-strain curves of basic model of CPFMincluding crack initiation, macroscopic failure and post failure.

4 Discussion

Two key aspects are aimed at in simulating rock mechanics experiments in this study: (1) achieving numerical results that closely match experimental findings, and (2) capturing accurately the fracture pattern, fracture growth, and coalescence that represents the correct stress distribution within the model. The first objective is achieved through parameter calibration, the second by modelling the microstructure. 0 compares the simulation results with experimental data, demonstrating that the first objective has been successfully met. In line with the second objective, Fig. 4 illustrates the effect of strain rate on the tensile-to-shear stress ratio in the numerical uniaxial test. As the strain rate increases, this ratio rises, leading to a larger region governed by the tensile stress mechanism. This behaviour aligns with experimental observations, where tensile fractures occur. While the simulated overall fracture pattern compares well with the microstructural observations, some quantitative microstructural properties of uniaxially deformed granite specimens do not closely agree with the numerical simulation results. We formulate the thesis that part of the discrepancy may be due to the free lateral motion in uniaxial experiments. Further investigations, in particular under triaxial deformation conditions, should complement the present results and test the formulated thesis.

5 Conclusion

This study explored the effect of time scale on the mechanical behaviour of Padang granite through conventional phase-field fracture modelling (CPFM) using COMSOL Multiphysics. CPFM enables precise simulations and analysis of rock mechanical behaviour by considering the response of multiple pre-existing cracks in rock specimens and investigating the relation between rock mechanical parameters and phase-field numerical parameters. This study emphasises the importance of

incorporating microstructural features to simulate strain rate effects in numerical simulations for a more comprehensive understanding of rock mechanics and failure mechanisms. These insights can enhance the design and interpretation of mechanical tests in geomechanical applications and help to develop temporal and spatial upscaling approaches.

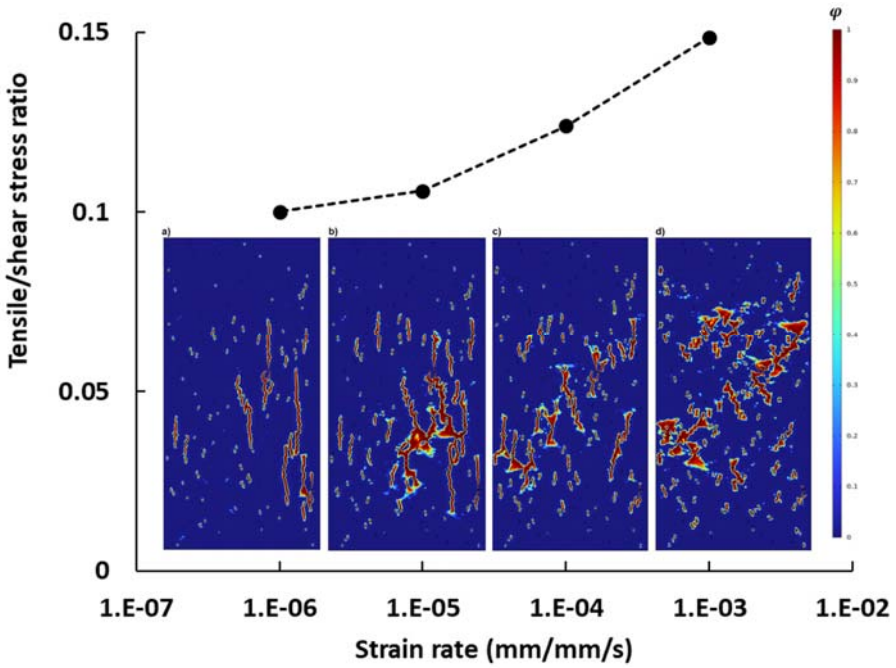


Fig. 4 Tensile to shear elements ratio after macroscopic failure in UCS tests at different strain rates and snapshots of the macroscopic failure pattern in numerical UCS tests at different strain rates: (a) strain rate $1 \cdot 10^{-6}$ s^{-1}, (b) strain rate $1 \cdot 10^{-5}$ s^{-1}, (c) strain rate $1 \cdot 10^{-4}$ s^{-1}, (d) strain rate $1 \cdot 10^{-3}$ s^{-1}.

Aspects of this work have been performed within the projects BeNuQuA (funding by SSM, Sweden) and AGENS (funded by the German Federal Ministry for Economic Affairs and Energy). We would like to thank for supporting our research.

References

Witte LC, Parvin S, Aydin M, Duda M, Backers T, Chehreh A (2025) Predictive capability of coupled rock behaviour – development of an experimentally based benchmark for numerical quality assurance (BeNuQuA). Ruhr University Bochum doi: 10.60517/F1881N35N.

Bieniawski Z (1967) Mechanism of brittle fracture of rock: part I - theory of the fracture process. International Journal of Rock Mechanics and Mining Sciences & Geomechanics Abstracts 4 (4): 405-406.

Bourdin B (2007) Numerical implementation of the variational formulation for quasi-static brittle fracture. Interfaces Free Bound 9 (3): 411–430.

Griffith AA (1921) The phenomena of rupture and flow in solids. Philosophical Transactions of the Royal Society 221: 163-197.

Miehe C, Hofacker M, Schaenzei LM, Aldakheel F (2015) Phase field modeling of fracture in multi-physics problems. Part II. Coupled brittle to ductile failure criteria and crack propagation in thermo-elastic-plastic solids. Computational Methods in Applied and Mechanical Engineering 294: 486-522.

Miehe C,Welschinger F,Hofacker M (2010a) Thermodynamically consistent phase-field models of fracture: variational principles and multi-field FE implementations, International Journal for Numerical Methods in Engineering 83 (10): 1273-1311.

Miehe C, Hofacker M,Welschinger F (2010b) A phase field model for rate-independent crack propagation: Robust algorithmic implementation based on operator splits. Computational Methods in Applied and Mechanical Engineering 199 (45): 2765-2778.

Molnar G, Doitrand A, Esteves R, Gravouil A (2020) Toughness or strength? Regularization in phase-field fracture explained by the coupled criterion, Theoretical and Applied Fracture Mechanics 109: 102736.

Zhao D, Yin B, Storm J, Kaliske M (2023) A phase-field formulation incorporating mode-dependent fracture toughness for fracture modeling in rock-like materials. Engineering Fracture Mechanics 289: 109345.